Variational Transition State Theory. Primary Kinetic Isotope Effects for Atom Transfer Reactions

Bruce C. Garrett and Donald G. Truhlar*

Contribution from the Department of Chemistry, University of Minnesota, Minneapolis, Minnesota 55455. *Received July 16, 1979*

Abstract: We consider the effect of variational determination of the location of the generalized transition state on the prediction of kinetic isotope effects for atom transfer reactions. Instead of choosing the transition state dividing surface on the basis of the conventional maximum energy criterion we use a maximum free energy criterion in which entropic effects compete with energetic effects. We consider several reactions with symmetric and nearly symmetric saddle points, loose saddle points, and intermediate cases. Numerical examples are based on model potential energy surfaces for three-body systems. The model potential energy surfaces are based on a modified and extended bond-energy, bond-order method that we have presented previously. We present examples involving isotopic substitution by ^2H, ^3H, ^{14}C, and ^{37}Cl for a wide range of temperatures. In some cases the results of the variational calculations essentially confirm the more readily used conventional transition state theory. However, this is not always the case. We show that the location of the variationally best transition state dividing surface is sometimes very sensitive to isotopic substitution. Furthermore, this sometimes leads to a large change in the predicted kinetic isotope effect.

I. Introduction

Transition-state theory (TST) is considered by many workers to provide a complete theory of kinetic isotope effects (KIEs) and it is the essentially universally applied tool for the interpretation of KIEs.[1-4] However, in some cases the accuracy of rate constants obtained using TST is expected to be poor, and there are indications that generalized TST may be more valid.[5-7] The present article is concerned with the application of the canonical variational theory (CVT),[5-7] one form of generalized TST, to primary kinetic isotope effects and with ascertaining the conditions which might lead to a serious breakdown of conventional TST for KIEs in gas-phase atom-transfer reactions.

The largest KIEs are primary H/D/T isotope effects. Such KIEs have been particularly well studied for many reactions.[3,4] Proton transfers[8-10] and hydrogen-atom transfers[5,11-13] are the simplest cases, and two key concepts have emerged in the application of TST to these reactions. The first is the relation of the primary KIE to symmetry of the transition state: larger isotope effects are usually interpreted as corresponding to more symmetric transition states.[2,8-10,12,14,15] The second is tunneling: larger KIEs than can be accounted for by TST with isotope-independent transmission coefficients even with symmetric transition states (e.g., $k_H/k_D \simeq 10$ for atom–diatom reactions at 300 K) are usually attributed to tunneling,[9,16] although of course tunneling may also play an important role when k_H/k_D is not larger than the maximum value that could possibly be accounted for without tunneling. Primary KIEs involving heavier isotopes have also been studied and are generally less than 1.2.[17,18]

In principle, TST should include a classical recrossing coefficient, a nonequilibrium correction factor, and a quantal correction factor, one or all of which may be defined so that TST becomes exact.[15,19] We here combine these effects into a single function of temperature called the transmission coefficient. In practice the transmission coefficient cannot be determined exactly. It is often assumed to be unity or at least independent of isotopic substitution, although isotope-dependent corrections seem to be required for proton transfer and hydrogen atom transfer reactions.[9,13,16] The fundamental assumption of TST is a classical one, namely, that all trajectories through the transition state, a dividing surface in configuration space or phase space separating reactants from products, cross the dividing surface but once and further that there is a quasi-equilibrium between reactants and systems at the dividing surface proceeding toward products.[20,21] Classically, TST for any choice of dividing surface provides an upper bound on the thermal rate constant.[22] The conventional version of TST is obtained if the dividing surface is placed at the highest energy point on the minimum energy path and perpendicular to the path of steepest descents away from this saddle point. In some cases there is another location of the dividing surface which yields a lower predicted thermal rate; in that case, in classical mechanics, the alternative dividing surface is crossed less frequently than the conventional one and is more consistent with the fundamental assumption of TST. In CVT one varies the location of the dividing surface to minimize the predicted thermal rate constant; this can be reformulated as a maximization of the free energy of activation as compared to maximization of the classical potential energy of activation in conventional TST. Although CVT is more consistent than conventional TST, it is not exact as applied here because (1) no attempt is made to estimate the extent of nonequilibrium or classical recrossing at the variational dividing surface; (2) for practical reasons one does not in general allow completely unconstrained variations of the dividing surface; (3) one calculates the generalized transition state partition function with a separable reaction coordinate and separable vibrations and rotation; (4) it is impossible to incorporate all quantum-mechanical effects into conventional or generalized TST. Regarding (2), in the present work we choose the dividing surface to be a surface in configuration space perpendicular to the path of steepest descents, and we choose the best such dividing surface for each temperature. In general there is no such surface that is not recrossed classically. One could attempt to improve upon the formalism employed here by using less constrained dividing surfaces in the CVT or one could go beyond the CVT by finding the best dividing surface for each total energy and total angular momentum or by attempting to estimate the amount of classical recrossing. In regard to (3) we note that we do include anharmonicity but our transition state energy levels are still not exact. Regarding (4), in the present work we calculate transmission coefficients in an attempt to estimate the dominant quantal effects on motion along a reaction coordinate which is assumed separable. We make no attempt to treat nonseparability of the reaction coordinate or vibrational nonadiabaticity which would alter the usual quantization of bound degrees of freedom of the transition state. Nonseparability and vibrational nonadiabaticity can also have a large effect on the dynamics in the tunneling regime.[23]

0002-7863/80/1502-2559$01.00/0

II. Theory and Calculational Details

The canonical variational theory formalism employed here is explained elsewhere.[6] In summary the generalized transition state theory rate constant with unit transmission coefficient for an atom–diatom reaction at temperature T for a dividing surface located a distance s from the saddle point is given by

$$k^{GT}(T,s) = \sigma \frac{k_B T}{h} \frac{Q^{GT}(T,s)}{\Phi^{R}_{rel}(T) Q^{R}_{int}(T)} e^{-V_{MEP}(s)/k_B T} \quad (1)$$

where σ is the symmetry factor, k_B is Boltzmann's constant, T is temperature, $\Phi^{R}_{rel}(T)$ and $Q^{R}_{int}(T)$ are the reactant relative translational partition function per unit volume and internal partition function, s is the reaction coordinate measured from $s = 0$ at the saddle point, $Q^{GT}(T,s)$ is the generalized transition state internal partition function, and $V_{MEP}(s)$ is the classical potential energy along the minimum-energy path at the dividing surface at s relative to the classical potential energy minimum of the reactants. Equation 1 can also be written

$$k^{GT}(T,s) = \frac{k_B T}{h} K^0 e^{-\Delta G^{GT,0}(T,s)/k_B T} \quad (2)$$

where K^0 is the reciprocal of the standard-state concentration and $\Delta G^{GT,0}(T,s)$ is the standard-state free-energy change in forming from reactants the generalized transition state located at s. For calculations, rotation and vibration are assumed separable, and we include Morse anharmonicity in stretching vibrational energies and quartic anharmonicity in bending vibrational energies. All vibrational and rotational partition functions are evaluated as quantum-mechanical sums with zeros of energy at the bottom of the local potential wells. The CVT rate constant with classical treatment of reaction-coordinate motion and other degrees of freedom quantized is the one that minimizes $k^{GT}(T,s)$ or maximizes $\Delta G^{GT,0}(T,s)$ with respect to s. The conventional TST rate constant with a transmission coefficient of unity is the one obtained by setting $s = 0$.

There are still some unsolved problems in trying to treat quantal corrections on the reaction-coordinate motion in a conventional or generalized TST framework.[5,24,25] These difficulties are of a fundamental nature because incorporating quantum effects into transition-state theory by quantizing the transition state and calculating a transmission coefficient $\kappa(T)$ based on a one-dimensional quantal treatment of the reaction-coordinate motion is valid only in a separable approximation. Nevertheless, in the present paper we include a $\kappa(T)$ of this type mainly for the purpose of indicating whether or not tunneling is important for a given reaction. For this purpose we calculate a semiclassical transmission probability $P^{SAG}(E_{rel})$ for relative translational energy E_{rel} for the ground-state adiabatic potential energy curve along the minimum-energy path. This potential-energy barrier is defined by

$$V^{AG}(s) = V_a(\alpha = 0,s) - V_a(\alpha = 0,s = -\infty) \quad (3)$$

where α denotes the set of quantum numbers for the bound degrees of freedom; the adiabatic potential curve is defined by

$$V_a(\alpha,s) = V_{MEP}(s) + \epsilon^{GT}_{int}(\alpha,s) \quad (4)$$

and $\epsilon^{GT}_{int}(\alpha,s)$ is the internal energy of the bound degrees of freedom for the generalized-transition-state dividing surface at s. In eq 3, $\alpha = 0$ denotes the ground state. In this article we restrict consideration to systems with collinear minimum energy paths; for such systems $\alpha = 0$ implies zero-point energies in the stretch and twofold degenerate bend and zero angular momentum in rotation and in translational orbital motion. In the present study we neglect curvature of the reaction coordinate in calculating $P^{SAG}(E_{rel})$. The vibrationally adiabatic, ground-state transmission coefficient for canonical variational theory is the ratio of the thermally averaged semiclassical transmission probability for $V^{AG}(s)$ to the thermal average of the classical transmission probability assumed by the uncorrected theory. Canonical variational theory with classical reaction coordinate motion assumes a step function rising to unity at E_{rel} equal to $V^{AG}[s = s_*^{CVT}(T)]$, where $s_*^{CVT}(T)$ denotes the value of the reaction coordinate at the location of the canonical variational transition state for the temperature T. Thus the semiclassical, vibrationally adiabatic, ground-state, zero-curvature transmission coefficient for canonical variational theory is

$$\kappa^{CVT/SAG}(T) = \frac{\int_0^\infty dE_{rel} P^{SAG}(E_{rel}) \exp(-E_{rel}/k_B T)}{\int_{V^{AG}[s_*^{CVT}(T)]}^\infty dE_{rel} \exp(-E_{rel}/k_B T)} \quad (5)$$

For brevity we do not include reminders in the superscript that we are using the minimum-energy path (MEP) and the zero-curvature (ZC) approximation in calculating the transmission coefficient. However, such a reminder may be useful if one compares the present treatment to others. Notice that the integration in the numerator extends from zero to infinity, indicating that barrier tunneling and nonclassical barrier reflection are included in $\kappa^{CVT/SAG}(T)$. Notice that $P^{SAG}(E_{rel})$ does not tend in the classical limit to a step function at E_{rel} equal to $V^{AG}[s_*^{CVT}(T)]$, but rather it tends to a step function at E_{rel} equal to the maximum of $V^{AG}(s)$. In the vibrationally adiabatic separable approximation, systems with energies between these two values would be classically transmitted at the canonical variational transition state but reflected at the vibrationally adiabatic barrier maximum. Thus $\kappa^{CVT/SAG}$ includes not only a semiclassical approximation to quantal tunneling and nonclassical reflection but also the effects of classical recrossing; all three effects are included in a vibrationally adiabatic separable approximation.

To calculate the transmission coefficient $\kappa^{CVT/SAG}(T)$ it is necessary to first obtain the ground-state adiabatic barrier $V^{AG}(s)$. The method for obtaining the potential energy, Morse parameters and energy levels for the stretching degree of freedom, and harmonic and quartic force constants, effective mass, and energy levels for the bending degree of freedom are given in ref 6. The ground-state adiabatic curve is then just the sum of the potential energy along the minimum-energy path and the ground-state energies of the stretch and twofold-degenerate bend. Values of $V^{AG}(s)$ were computed at intervals along the reaction coordinate and then represented by spline fits. The spline fits were then used in obtaining $P^{SAG}(E_{rel})$. The techniques used for the semiclassical approximation to the quantal transmission probability for a given barrier and for the integration in eq 5 are explained elsewhere.[26]

To calculate the canonical variational rate constant we used the free-energy formulation indicated in eq 2. Details of the calculation of the free-energy change $\Delta G^{GT,0}(T,s)$ and location of its maximum can be found in ref 6.

To interpret the results we will divide the effects into energetic and entropic ones. Although the bound degrees of freedom are quantized, we still find it most illuminating to consider the energetic contribution to the free energy of the dividing surface to be the energy at the minimum of the classical potential energy for the dividing surface and to consider all other effects (i.e., changes in partition functions with the zero of energy at the classical potential energy minimum) to be entropic effects. Thus entropic effects in this context reflect any changes in force constants and moments of inertia, not just those that reflect a change in the effective number of occupied

states. An alternative interpretation would be to discuss changes in zero-point energies as an energetic effect. The present mode of discussion, however, allows for a clearer understanding of the factors which make the variational theory differ from the conventional.

III. Systems Studied

We selected a representative set of systems based on our experience[6,7] applying the CVT to thermal rate constants without isotopic substitution. In all cases the potential-energy surface is mimicked by an extended modified bond-energy bond-order method (BEBO) (patterned on the methods of Johnston and Parr[27] and Mayer, Schieler, and Johnston[28]) which is explained elsewhere.[6,7] Although this model does not predict quantitatively accurate potential-energy surfaces (no practical model does), it does predict realistic ones which are widely used for the correlation and prediction of kinetic data.[29] For our purposes, the BEBO method is sufficient to generate a set of realistic surfaces with a simple physical interpretation in order to survey the effects of varying the location of the dividing surface. The data used for the present BEBO calculations are tabulated elsewhere.[27,30]

To emphasize that the present study is for model reactions, we consider the BEBO potential surface for C + HC. The physical model employed in the BEBO method is most appropriate for a singly valent doublet atom reacting with a closed shell singlet molecule, but there is no three-body reaction with masses 12, 1, and 12 that has a singly valent doublet atom approaching a closed-shell singlet diatom. The BEBO potential surface for C + HC has a 12.7 kcal/mol barrier and is reasonably representative of the three-body part of the CH_3 + H-CH_3 reaction. However, the C + HC model considered here is treated consistently as a three-body reaction and simply represents the interesting case of a hydrogen atom transferred in a symmetric way between two heavier fragments on a potential surface with a simple symmetric barrier. Similar remarks apply to the other cases considered here. Taken as a group the 19 model reactions and isotopic analogues considered here span a wide range of combinations of masses and realistic surface types. Thus the present work provides a survey of possibilities which should be considered in assessing the importance of variational optimization of the transition-state dividing surface for kinetic isotope effects in three-body reactions. The results are also relevant to many atom-transfer reactions involving more than three atoms because in many cases the three-body part involved in bond breaking and bond making plays the dominant role.

IV. Results

A survey of hydrogen atom isotope effects for 17 reactions is provided in Table I. As an indication of the importance of variational determination of the location of the generalized transition state, we have tabulated the ratio $k_D^{\ddagger}(T)/k_D^{CVT}(T)$ of conventional to canonical variational transition state theory rate constants for the deuterium-substituted reactions. Also tabulated are the KIEs predicted by conventional transition state theory, canonical variational theory, and canonical variational theory with the semiclassical vibrationally adiabatic ground-state transmission coefficient. The table is arranged with the systems with the most symmetrically located saddle points entered first. Tables II and III contain analogous results for the carbon-12/14 and chlorine-35/37 isotope effects. To help explain the effects of generalized transition state theory upon KIEs, Table IV contains details for some of the reactions of the generalized transition state located at the saddle point and also at the CVT transition state for 600 K. For each generalized transition state in this table we give the bond order n_{AB} of the new bond, the harmonic frequencies ω_e and ω_b of the stretching and bending degrees of freedom, respectively, values

Table I. Deuterium Kinetic Isotope Effects at 300, 600, and 1000 K[a]

system A + BC	T, K	$k_D^{\ddagger}/k_D^{CVT}$	$k_H^{\ddagger}/k_D^{\ddagger}$	k_H^{CVT}/k_D^{CVT}	$k_H^{CVT/SAG}/k_D^{CVT/SAG}$
C + HC	300	3.79	4.83	0.74	0.93
	600	2.34	2.36	0.90	0.95
	1000	2.15	1.76	0.92	0.94
O + HO	300	24.65	9.40	0.74	0.77
	600	5.78	3.19	0.89	0.90
	1000	3.77	2.06	0.93	0.93
C + H_2	300	2.98	4.94	1.85	4.46
	600	1.80	2.69	1.71	2.17
	1000	1.58	1.94	1.54	1.68
^{14}C + H_2	300	3.08	4.93	1.88	4.49
	600	1.84	2.70	1.73	2.19
	1000	1.60	1.95	1.56	1.70
H + HO	300	1.48	1.01	0.79	1.10
	600	1.18	1.27	1.14	1.23
	1000	1.09	1.33	1.25	1.29
C + HO	300	1.25	0.96	1.00	1.16
	600	1.10	1.00	1.05	1.09
	1000	1.05	1.03	1.02	1.03
C + FH	300	1.02	8.36	5.63	7.42
	600	1.04	2.85	2.16	2.33
	1000	1.07	1.81	1.39	1.45
Cl + CH	300	1.00	5.48	4.79	5.24
	600	1.01	2.36	1.96	1.93
	1000	1.03	1.71	1.28	1.19
Br + NH	300	1.02	7.85	6.70	6.56
	600	1.04	2.86	2.07	1.92
	1000	1.07	1.94	1.16	1.05
H + HF	300	1.07	0.82	0.81	0.89
	600	1.13	1.12	1.13	1.17
	1000	1.19	1.24	1.25	1.28
Li + HO	300	1.11	3.67	3.44	3.50
	600	1.15	1.89	1.81	1.83
	1000	1.21	1.39	1.34	1.36
Cl + HO	300	1.53	1.39	1.30	1.34
	600	1.73	1.19	1.14	1.19
	1000	1.93	1.11	1.07	1.10
Li + HI	300	1.41	2.02	1.92	1.97
	600	1.77	1.39	1.29	1.27
	1000	2.31	1.19	1.10	1.18
Cl + ClH	300	1.22	7.30	7.30	7.60
	600	1.36	2.73	2.73	2.78
	1000	1.49	1.89	1.90	1.92
Cl + IH	300	1.32	4.80	4.79	4.91
	600	1.50	2.23	2.23	2.26
	1000	1.67	1.71	1.70	1.68
F + ClH	300	1.56	7.30	7.29	7.53
	600	1.85	2.73	2.73	2.79
	1000	2.12	1.89	1.89	1.93
I + IH	300	1.36	4.81	4.80	4.93
	600	1.55	2.23	2.23	2.26
	1000	1.73	1.72	1.70	1.67
I + HBr	300	1.94	1.23	1.20	1.26
	600	2.42	1.10	1.09	1.14
	1000	2.91	1.05	1.04	1.08

[a] For reactions with more than one hydrogen, the isotope effect is for replacement of both hydrogens with deuteriums.

$V_{MEP}(s)$ of the potential along the minimum-energy path relative to the bottom of the reactant potential well, and the value $V^{AG}(s)$ of the vibrationally adiabatic potential curve relative to the zero-point energy of the reactants. Also tabulated for 600 K are the ratios of the conventional and CVT partition functions for the bending, rotational, and stretching degrees of freedom, the ratio of the Boltzmann factors for the potential energy at the saddle point and at the CVT transition state, as well as the ratio of conventional and CVT rate constants. This ratio of rate constants is the product of the previous four factors, and is also given for temperatures of 200 and 1000 K.

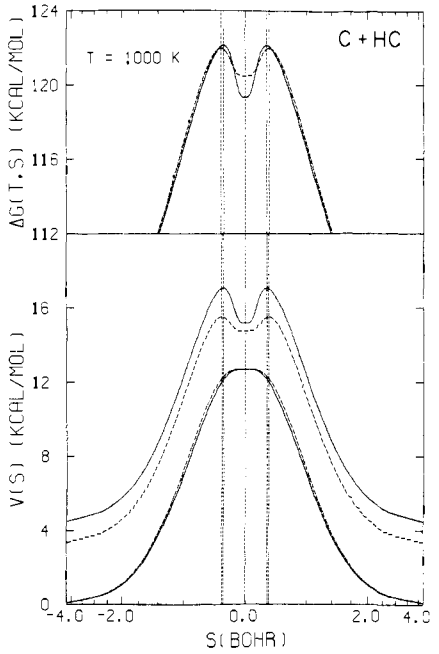

Figure 1. Classical potential energy barrier, ground-state zero-angular-momentum adiabatic potential energy barrier, and generalized free energy of activation curves as functions of reaction coordinate s for the reaction C + HC → CH + C and its isotopic variant C + DC → CD + C. For all three types of curves the solid curves are for the H isotope and the dashed curves are for the D isotope. The lowest pair of curves are the classical potential energy barriers with zero of energy taken at the bottom of the reactant well. These curves differ slightly for the two isotopic variants because the reaction coordinate is measured along the minimum-energy path for the corresponding isotope-dependent scaled and skewed coordinate system in each case. The two higher curves on the lower portion of the figure are the ground-state, zero-angular-momentum adiabatic potential curves $V_a(\alpha = 0,s)$. The two curves in the upper portion of the figure are the generalized free energy of activation curves for a temperature of 1000 K and a standard state of 1 cm³/molecule. Note that the ground-state adiabatic curves are the free energy of activation curves for a temperature of 0 K. The dotted vertical line at $s = 0$ indicates the saddle point; the dotted lines in the lower panel indicate the maxima in the ground-state, zero-angular-momentum adiabatic potential curves, and the dotted lines in the upper panel indicate the maxima in the free energy of activation curves for 1000 K. For this symmetric reaction as well as the symmetric O + HO reaction there are two identical maxima in the ground-state adiabatic curves and the free energy of activation curves. For each of Figures 1-10, the reaction A + BC is thermoneutral or endothermic, and the curves are plotted as a function of the square root of the distance along the reaction coordinate. The range of reaction coordinate was chosen such that the values of the ground-state, zero-angular-momentum adiabatic potential curves at the boundaries differ from the asymptotic values by less than a specified amount. For this figure, the ground-state, zero-angular-momentum adiabatic potential curves at the boundaries differ from the asymptotic values by less than 1.5×10^{-4} hartree.

Figures 1-10 compare the potential-energy curves, adiabatic potential curves, and generalized free energy of activation curves at $T = 1000$ K for ten reactions (solid curves) and their deuterium-substituted variants (dashed curves). The dashed vertical lines indicate the location of the saddle point ($s = 0$), the maxima of the adiabatic potential curves, and the maxima of the free-energy curves.

Tables V and VI give further details of the factors which contribute to the kinetic isotope effects for the reactions contained in Table IV. These factors are described in section V.

Table VII is a test of the Swain-Schaad equation. This equation was originally derived for reactions of the form

$$A + HX \rightarrow AH + X$$

where at least one of X and A is heavy, and H is ^{1}H, D, or T. Using conventional transition state theory and assuming that all differences except zero-point energy are negligible, Swain et al.[31] obtained the approximate relation

$$k_{^1H}/k_T \cong (k_{^1H}/k_D)^{1.442} \equiv (k_{^1H}/k_T)_{SS} \quad (6)$$

The identity defined by the second relationship sign in (6) will be called the Swain-Schaad prediction of $k_{^1H}/k_T$. Notice in

Table II. Carbon-14 Kinetic Isotope Effects at 300, 600, and 1000 K[a]

system A + BC	T, K	$k_{C^*}^{\ddagger}/k_{C^*}^{CVT}$	$k_C^{\ddagger}/k_{C^*}^{\ddagger}$	$k_C^{CVT}/k_{C^*}^{CVT}$	$k_C^{CVT/SAG}/k_{C^*}^{CVT/SAG}$
C* + HC	300	27.95	0.981	1.113	1.108
	600	6.60	0.998	1.077	1.075
	1000	4.35	1.002	1.063	1.062
C* + HC*	300	30.52	0.986	1.221	1.258
	600	7.01	1.003	1.149	1.157
	1000	4.58	1.004	1.122	1.125
Cl + C*Cl	300	1.56	1.128	1.010	1.012
	600	1.58	1.084	0.999	1.001
	1000	1.64	1.074	0.996	0.999
C* + H_2	300	8.07	1.013	1.029	1.027
	600	2.86	1.012	1.020	1.020
	1000	2.00	1.012	1.016	1.016
C* + D_2	300	3.08	1.012	1.046	1.034
	600	1.84	1.015	1.032	1.029
	1000	1.60	1.016	1.028	1.026
C* + HO	300	1.20	1.080	1.064	1.052
	600	1.07	1.063	1.055	1.052
	1000	1.03	1.056	1.052	1.051
C* + FH	300	1.62	1.008	1.075	1.066
	600	1.42	1.026	1.066	1.062
	1000	1.44	1.031	1.063	1.060
Cl + C*H	300	1.22	1.050	1.120	1.116
	600	1.29	1.045	1.103	1.093
	1000	1.43	1.042	1.093	1.076
O + ClC*	300	1.19	1.126	1.126	1.128
	600	1.31	1.081	1.081	1.081
	1000	1.42	1.070	1.070	1.072

[a] k_C is the rate constant with all carbon atoms ^{12}C; k_{C^*} is the rate constant with those carbon atoms marked C* replaced by ^{14}C.

Table III. Chlorine Kinetic Isotope Effects at 300, 600, and 1000 K[a]

system A + BC	T, K	$k_{^{37}Cl}^{\ddagger}/k_{^{37}Cl}^{CVT}$	$k_{^{35}Cl}^{\ddagger}/k_{^{37}Cl}^{\ddagger}$	$k_{^{35}Cl}^{CVT}/k_{^{37}Cl}^{CVT}$	$k_{^{35}Cl}^{CVT/SAG}/k_{^{37}Cl}^{CVT/SAG}$
Cl* + CCl	300	1.79	1.000	1.026	1.024
	600	1.75	1.002	1.022	1.022
	1000	1.80	1.002	1.021	1.021
Cl* + CCl*	300	1.80	1.007	1.038	1.038
	600	1.76	1.005	1.033	1.033
	1000	1.82	1.004	1.031	1.031
Cl* + CH	300	1.16	0.996	1.003	1.004
	600	1.23	1.000	1.007	1.007
	1000	1.38	1.001	1.009	1.008
Cl* + HO	300	1.64	1.004	1.005	1.005
	600	1.81	1.007	1.007	1.007
	1000	2.01	1.007	1.008	1.008
O + Cl*C	300	1.19	1.001	1.001	1.002
	600	1.31	1.003	1.003	1.003
	1000	1.42	1.003	1.003	1.003
Cl* + Cl*H	300	1.22	0.990	0.990	0.990
	600	1.36	0.998	0.998	0.998
	1000	1.49	1.000	1.000	1.000
Cl* + IH	300	1.32	0.994	0.994	0.994
	600	1.50	0.999	0.999	0.999
	1000	1.69	0.999	1.000	1.003
F + Cl*H	300	1.56	0.996	0.996	0.996
	600	1.84	1.000	1.000	1.000
	1000	2.11	1.000	1.000	1.001

[a] $k_{^{35}Cl}$ is the rate constant with all chlorine atoms ^{35}Cl; $k_{^{37}Cl}$ is the rate constant with those chlorine atoms marked Cl* replaced by ^{37}Cl.

Table IV. Properties of Generalized Transition States and Ratios of Conventional and CVT Partition Functions

system	saddle-point properties					CVT transition state properties (T = 600 K)					T = 600 K					T = 200 K	T = 1000 K
											$Q^{\ddagger}/Q^{CVT}$						
A + BC[a]	n_{AB}[b]	$\hbar\omega_c$,[c] cm^{-1}	$\hbar\omega_b$,[d] cm^{-1}	V_{MEP},[e] kcal/mol	$V^{AG}(s=0)$,[f] kcal/mol	n_{AB}[b]	$\hbar\omega_c$,[c] cm^{-1}	$\hbar\omega_b$,[d] cm^{-1}	V_{MEP},[e] kcal/mol	$V^{AC}[s=s_*^{CVT}(T)]$,[f] kcal/mol	bends[g]	rot.[h]	stretch[i]	$e^{\Delta V/k_BT}$	$k^{\ddagger}/k^{CVT}$	$k^{\ddagger}/k^{CVT}$	$k^{\ddagger}/k^{CVT}$
C + HC	0.500	621	508	12.67	10.94	0.63	2355	498	12.14	12.8	0.96	0.99	10.06	0.64	6.12	116	4.10
C + DC	0.500	621	367	12.67	11.60	0.62	1523	360	12.19	12.4	0.96	0.99	3.67	0.67	2.34	7.03	2.15
^{14}C + HC	0.500	600	507	12.67	10.91	0.62	2370	497	12.16	12.8	0.96	0.99	10.68	0.65	6.60	139	4.35
^{14}C + H^{14}C	0.500	575	506	12.67	10.89	0.62	2375	497	12.17	12.9	0.96	0.99	11.28	0.66	7.01	157	4.58
Cl + CCl	0.500	305	80	3.58	3.06	0.67	624	77	3.37	3.3	0.95	0.98	2.19	0.84	1.71	1.93	1.77
Cl + ^{14}CCl	0.500	305	75	3.58	3.11	0.67	580	73	3.37	3.3	0.95	0.98	2.01	0.84	1.58	1.66	1.64
^{37}Cl + CCl	0.500	301	80	3.58	3.05	0.66	626	77	3.37	3.3	0.95	0.98	2.23	0.84	1.75	1.99	1.80
^{37}Cl + C^{37}Cl	0.500	297	79	3.58	3.05	0.67	623	77	3.37	3.3	0.95	0.98	2.25	0.84	1.76	2.00	1.81
C + H$_2$	0.546	1759	662	14.60	12.88	0.40	3103	673	13.93	14.1	1.04	0.96	4.94	0.57	2.84	22.7	1.99
C + D$_2$	0.546	1246	471	14.60	13.36	0.42	2037	479	14.12	14.0	1.04	0.97	2.67	0.67	1.80	5.15	1.58
^{14}C + H$_2$	0.546	1760	662	14.60	12.88	0.40	3109	672	13.94	14.1	1.04	0.96	4.95	0.58	2.86	23.2	2.00
H + HO	0.620	3260	603	10.79	11.91	0.71	3704	586	10.63	12.3	0.94	0.95	1.68	0.88	1.32	2.72	1.15
D + DO	0.620	2274	428	10.79	11.41	0.69	2547	419	10.69	11.7	0.96	0.96	1.38	0.92	1.18	1.87	1.09
C + FH	0.811	1240	272	41.54	38.22	0.73	1633	300	41.10	38.4	1.22	0.99	1.65	0.69	1.37	1.76	1.39
C + FD	0.811	1033	212	41.54	39.35	0.78	1043	220	41.48	39.3	1.07	1.00	1.01	0.95	1.04	1.02	1.07
^{14}C + FH	0.811	1225	271	41.54	38.20	0.73	1662	299	41.07	38.4	1.23	0.98	1.74	0.68	1.42	1.93	1.44
Cl + CH	0.852	761	198	30.28	27.81	0.78	954	222	29.90	27.8	1.25	0.99	1.35	0.73	1.22	1.15	1.37
Cl + CD	0.852	719	156	30.28	28.72	0.84	705	160	30.26	28.7	1.05	1.00	0.98	0.99	1.01	1.00	1.03
Cl + ^{14}CH	0.852	746	194	30.28	27.81	0.77	988	220	29.86	27.8	1.27	0.99	1.45	0.71	1.29	1.25	1.43
^{37}Cl + CH	0.852	757	198	30.28	27.81	0.78	958	222	29.89	27.8	1.25	0.99	1.37	0.72	1.23	1.16	1.38
Cl + HO	0.957	3020	171	8.65	8.16	0.86	3067	258	8.24	8.1	1.99	1.20	1.06	0.71	1.81	1.59	2.00
Cl + DO	0.957	2162	122	8.65	8.22	0.87	2179	182	8.29	8.1	1.92	1.20	1.02	0.74	1.73	1.45	1.93
^{37}Cl + HO	0.957	3018	171	8.65	8.16	0.86	3066	258	8.24	8.1	1.99	1.20	1.06	0.71	1.81	1.60	2.00
O + ClC	0.981	861	36	30.65	30.79	0.95	849	44	30.44	30.6	1.43	1.11	0.98	0.84	1.31	1.14	1.42
O + Cl^{14}C	0.981	861	35	30.65	30.86	0.95	849	44	30.44	30.6	1.43	1.11	0.98	0.84	1.31	1.14	1.42
O + ^{37}ClC	0.981	854	35	30.65	30.79	0.95	842	44	30.44	30.6	1.43	1.11	0.98	0.84	1.31	1.14	1.42
Li + Hl	0.991	1390	172	18.85	18.07	0.85	1503	288	17.91	17.6	2.58	1.42	1.15	0.45	1.91	1.38	2.51
Li + Dl	0.991	1041	125	18.85	18.37	0.90	1077	195	18.15	17.9	2.22	1.36	1.05	0.56	1.77	1.31	2.31
Cl + ClH	0.992	563	69	49.14	45.91	0.98	558	92	48.90	45.7	1.66	1.02	0.99	0.81	1.36	1.17	1.49
Cl + ClD	0.992	564	52	49.14	47.05	0.98	560	69	48.90	46.8	1.63	1.03	0.99	0.81	1.36	1.17	1.49
^{37}Cl + ^{37}ClH	0.992	548	69	49.14	45.89	0.98	543	91	48.90	45.7	1.66	1.02	0.99	0.81	1.36	1.17	1.49

[a] In all cases reaction occurs with the atom written first in the diatomic. For homonuclear diatomics the rate calculated is the sum of the reaction rates with both ends. [b] Bond order of the new bond. [c] Planck's constant times the vibrational frequency for the stretching degree of freedom. [d] Planck's constant times the vibrational frequency for a single bending degree of freedom. [e] Classical potential energy relative to zero at the bottom of the asymptotic reactant vibrational well. [f] Value of the ground-state adiabatic potential curve relative to zero at the zero-point vibrational energy of reactants. [g] Square of the ratio of bending partition functions. [h] Ratio of rotational partition functions. [i] Ratio of stretching partition functions. [j] $\exp\{-[V_{MEP}(s=0) - V_{MEP}(s=s_*^{CVT})]/k_BT\}$.

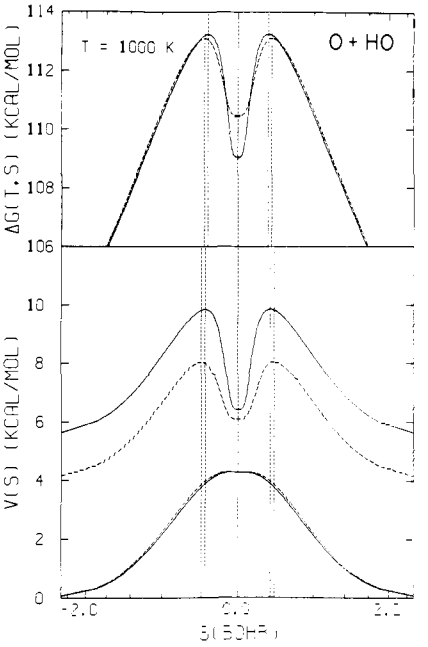

Figure 2. Same as Figure 1 except for the reactions O + HO → OH + O and O + DO → OD + O. For this figure the values of the adiabatic potential curves at the boundaries differ from their asymptotic values by less than 1.5×10^{-4} hartree.

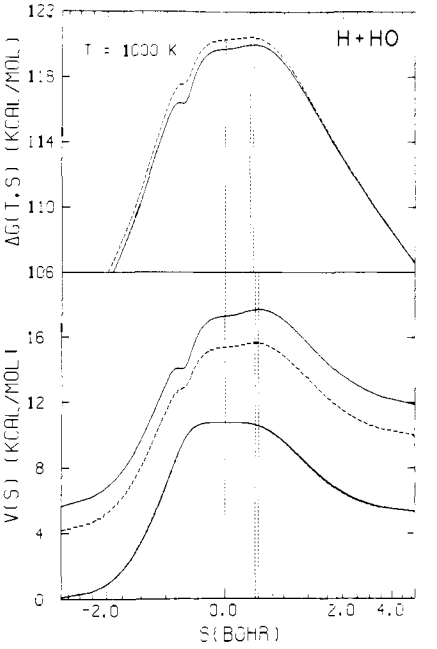

Figure 4. Same as Figure 3 except for the reactions H + HO → H_2 + O and D + DO → D_2 + O. For this figure the values of the adiabatic potential curves at the boundaries differ from their asymptotic values by less than 1.5×10^{-4} hartree.

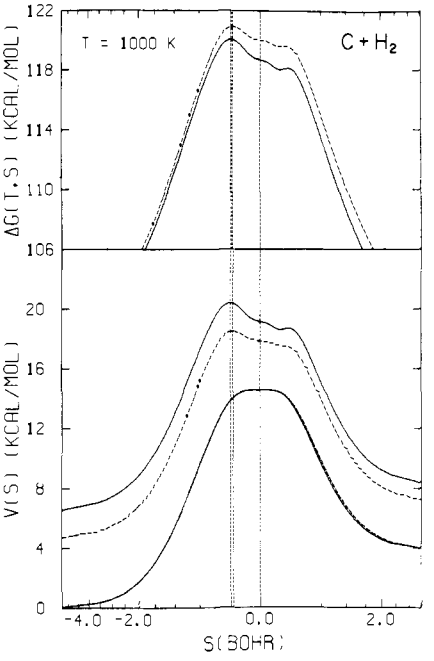

Figure 3. Same as Figure 2 except for the reactions C + H_2 → CH + H and C + D_2 → CD + D. For this figure the values of the adiabatic potential curves at the boundaries differ from their asymptotic values by less than 1.5×10^{-4} hartree.

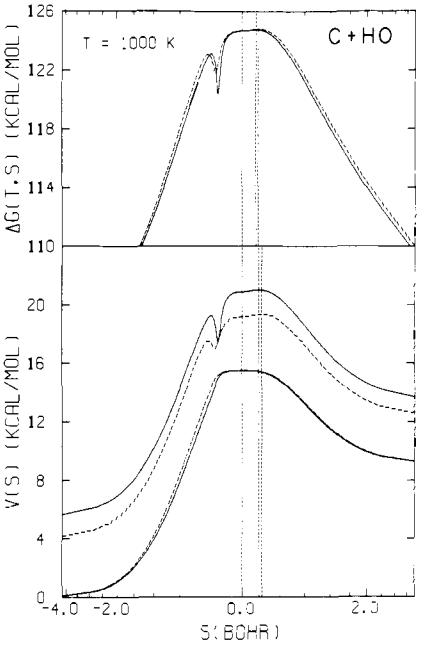

Figure 5. Same as Figure 4 except for the reactions C + HO → CH + O and C + DO → CD + O. For this figure the values of the adiabatic potential curves at the boundaries differ from their asymptotic values by less than 1.5×10^{-4} hartree.

particular that tunneling was neglected in the argument leading to (6). Table V presents tritium–protium isotope effects calculated by the three theories considered here and in each case compares them to the prediction of the Swain–Schaad relation.

V. Discussion

The first two reactions in Table I show dramatic effects of the variational optimization of the location of the generalized transition state. For example, for C + HC at 300 K, the variational optimization lowers the rate constant by a factor of 24.7. In contrast the rate constant for C + DC is lowered by "only" a factor of 3.8. The ratio of these changes is larger than the conventionally predicted KIE of 4.8; hence the CVT with unit transmission coefficient predicts an inverse isotope effect. Inclusion of a semiclassical tunneling correction based on the ground-state adiabatic potential curve changes the prediction to a value close to unity. A more accurate tunneling correction might well restore the normal isotope effect since the vibrationally adiabatic method with zero curvature is known[24,32-34] to sometimes underestimate the extent of tunneling. The quantitative prediction that the isotope effect in the absence of tunneling would actually be inverse may also be sensitive to the details of the potential-energy surface. But one quali-

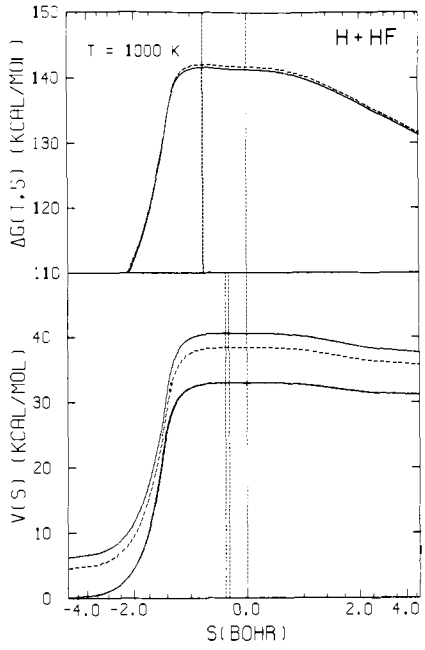

Figure 6. Same as Figure 5 except for the reactions H + HF → H_2 + F and D + DF → D_2 + F. For this figure the values of the adiabatic potential curves at the boundaries differ from their asymptotic values by less than 1.5×10^{-4} hartree.

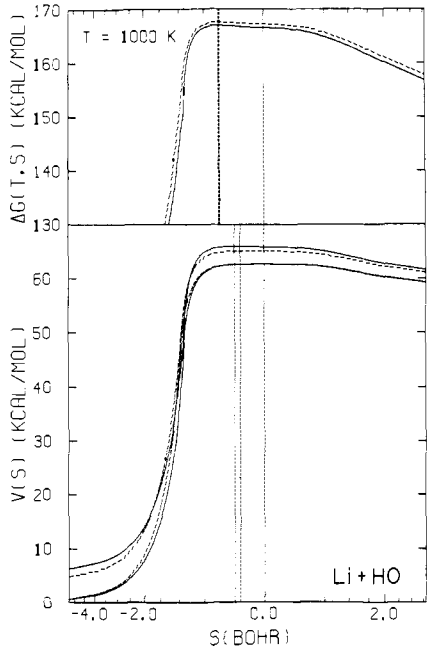

Figure 7. Same as Figure 6 except for the reactions Li + HO → LiH + O and Li + DO → LiD + O. For this figure the values of the adiabatic potential curves at the boundaries differ from their asymptotic values by less than 1.0×10^{-3} hartree.

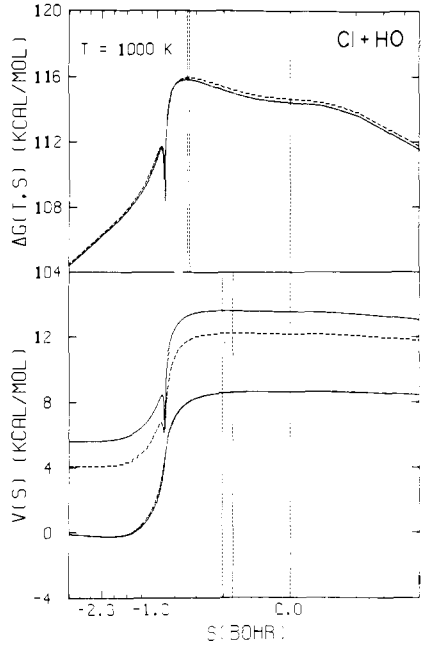

Figure 8. Same as Figure 7 except for the reactions Cl + HO → ClH + O and Cl + DO → ClD + O. For this figure the values of the adiabatic potential curves at the boundaries differ from their asymptotic values by less than 3×10^{-4} hartree.

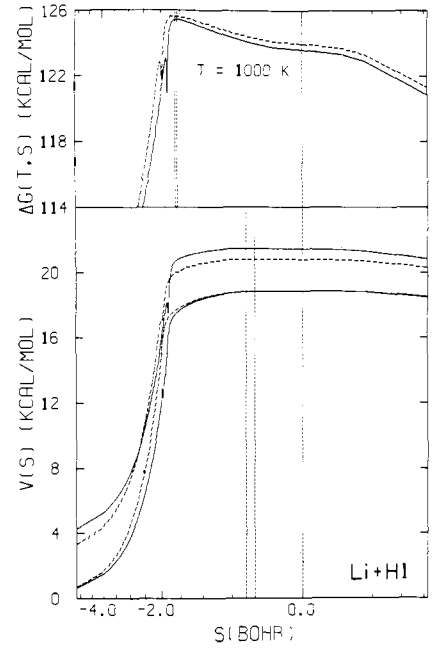

Figure 9. Same as Figure 8 except for the reactions Li + HI → LiH + I and Li + DI → LiD + I. For this figure the values of the adiabatic potential curves at the boundaries differ from their asymptotic values by less than 1.0×10^{-3} hartree.

tative fact is very clear, namely, that variation optimization of the location of the generalized transition state can have large effects on KIEs.

The fact that the change in the KIE is larger for the first two reactions in Table I than any of the others can be explained in terms of the effect of skew angle on the location of the variational transition state. In our general surveys of the effects on predicted rate constants of variational determination of generalized transition state locations, we have found that the largest effects of variational location of the generalized transition state are associated with reactions with symmetric and nearly symmetric saddle points, and the effects in such cases are dominated by the stretching degree of freedom.[6,7] Small skew angles are associated with a light atom being transferred between two heavy subsystems.[35] In such a case, if coordinates are not scaled, the reduced mass associated with the stretching degree of freedom increases greatly as the system proceeds to a symmetric or nearly symmetric geometry. Alternatively, if the coordinates are all scaled to the same reduced mass, the force constant decreases for symmetric or nearly symmetric geometries. In either coordinate system, the stretching frequency is much smaller for symmetric or nearly symmetric geometries than for reactants. Consider, as an example, the reaction C + HC. The stretching vibration is initially a hydride vibration with $\omega_e = 2912$ cm^{-1}. At the symmetric saddle point,

Table V. Factors Contributing to Deuterium Kinetic Isotope Effects at 600 K

isotope effect	translation[a]	rotation[b]	stretch[c]	bend[d]	energy[e]	net[f]
C + HC/C + DC	1.05[g]	1.84	2.50	0.48	1.00	2.36
	1.05[h]	1.85	0.92	0.49	1.04	0.90
C + H_2/C + D_2	2.31	1.10	2.36	0.45	1.00	2.69
	2.31	1.12	1.27	0.45	1.17	1.71
H + HO/D + DO	2.63	1.03	1.04	0.45	1.00	1.27
	2.63	1.05	0.86	0.46	1.05	1.14
C + FH/C + FD	1.03	1.60	2.89	0.60	1.00	2.85
	1.03	1.63	1.78	0.53	1.38	2.16
Cl + CH/Cl + CD	1.08	1.52	2.33	0.62	1.00	2.36
	1.08	1.53	1.69	0.52	1.35	1.96
Cl + HO/Cl + DO	1.06	1.87	1.20	0.50	1.00	1.19
	1.06	1.86	1.16	0.48	1.04	1.14
Li + HI/Li + DI	1.00	1.89	1.41	0.52	1.00	1.39
	1.00	1.82	1.28	0.45	1.23	1.29
Cl + ClH/Cl + ClD	1.02	1.69	2.73	0.58	1.00	2.73
	1.02	1.72	2.73	0.57	1.00	2.73

[a] $\Phi_{rel,D}^{R}(T)/\Phi_{rel,H}^{R}(T)$. [b] $Q_{rot,H}^{GT}(T,s_H)Q_{rot,D}^{R}(T)/Q_{rot,D}^{GT}(T,s_D)Q_{rot,H}^{R}(T)$. [c] $Q_{str,H}^{GT}(T,s_H)Q_{str,D}^{R}(T)/Q_{str,D}^{GT}(T,s_D)Q_{str,H}^{R}(T)$. [d] $[Q_{b,H}^{GT}(T,s_H)]^2/[Q_{b,D}^{GT}(T,s_D)]^2$. [e] $\exp\{[V_{MEP}(s_D) - V_{MEP}(s_H)]/k_BT\}$; for $s_H = s_D = 0$ this factor is unity. [f] $k_H^{GT}(T,s_H)/k_D^{GT}(T,s_D)$. [g] Upper entries are for the conventional location of the dividing surface, i.e., $s_H = s_D = 0$. [h] Lower entries are for the canonical variational location of the dividing surface, i.e., $s_H = s_{*,H}^{CVT}(T)$, $s_D = s_{*,D}^{CVT}(T)$.

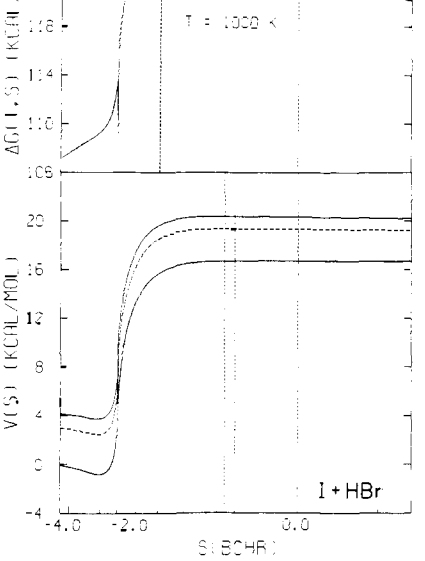

Figure 10. Same as Figure 9 except for the reactions I + HBr → IH + Br and I + DBr → ID + Br. For this figure the values of the adiabatic potential curves at the boundaries differ from their asymptotic values by less than 1.5×10^{-4} hartree.

the hydrogen is stationary and the reduced mass for the bound stretching vibration is controlled by the C-C moiety; as a consequence ω_e is reduced to 621 cm^{-1} (see Table IV). For C + DC, ω_e is reduced from 2138 cm^{-1} for reactants to 621 cm^{-1} at the saddle point. Figures 1 and 2 show that the shapes of the generalized free energy of activation curves are not sensitive to temperature in these cases. Thus the generalized free energy of activation curves may be explained in terms of the ground state vibrationally adiabatic potential curves, which in turn are easily explained in terms of ω_e as a function of reaction coordinate. When ω_e is greatly reduced, the entropy is increased (see last paragraph of section II). The entropy increase tends to increase the equilibrium flux through a generalized transition state dividing surface and to compete with the energy increase which occurs on proceeding to symmetric configurations. As a result the variationally best generalized transition state is located at the best compromise location (location of maximum free energy) rather than at the symmetric saddle point (location of maximum classical potential energy). Since the decrease in ω_e for the stretching vibration is 2291 cm^{-1} for C + HC but only 1517 cm^{-1} for C + DC, the entropic effect competes with the energetic effect more easily in the former case, and the variational lowering of the predicted rate constant is greater for the hydride than for the deuteride. At their variational transition states the values of ω_e are 2355 cm^{-1} for C + HC and 1523 cm^{-1} for C + DC (see Table IV). As compared to reactants this represents lowerings of 557 and 615 cm^{-1}, respectively, and the lowerings are actually ordered opposite to their values at the conventional transition state. This invalidates the simple conventional interpretation of the isotope effect in this case. In summary, we expect the variational location of the generalized transition state for symmetric hydrogen-atom transfers to be dominated by competition between the energetic effect and the entropy of the stretching degree of freedom. Since the skew angle is smaller for H transfer than D transfer, we expect a greater entropic effect in the former case. Thus conventional transition state theory, which locates the dividing surface entirely based on the energetic criterion, is expected to overestimate the ratio k_H/k_D, unless there is a competing error caused by tunneling.

It is interesting to notice the role of the bending frequency at the variational transition state on the canonical variational prediction that the isotope effect for the model reaction C + HC is inverse in the absence of quantum effects on reaction-coordinate motion. The role of the bending frequency in proton-transfer reactions has been widely discussed (see, e.g., ref 10, pp 27–30, and ref 15, pp 242–244) in terms of conventional transition state theory. In the example of C + HC with the present model potential surface the bending frequencies for the conventional and variational (600 K) transition states are 508 and 498 cm^{-1}, respectively. The same quantities for C + DC are 367 and 360 cm^{-1}. In proceeding to the conventional dividing surface, the stretching frequency decreases 2291 cm^{-1} for H and 1517 cm^{-1} for D. This contributes a factor of about $\exp[(2291 - 1517)/2k_BT] = 2.5$ to k_H/k_D. Similarly, in the low-temperature harmonic approximation, the bend would contribute $\exp[-(508 - 367)/k_BT] = 0.7$. Calculating the effect of the bend accurately yields 0.5. Since the translational partition function is almost the same for the two isotopic variations, the conventional prediction of k_H/k_D is essentially a product of three factors: 2.5 from the stretch, 0.5 from the bend, and 1.8 from reactant rotation. In general, variational optimization of the location of the generalized-transition-state dividing surface will decrease the effect on the KIE of the

Table VI. Factors Contributing to Heavy-Atom Kinetic Isotope Effects at 600 K

isotope effect	translation[a]	rotation[b]	stretch[c]	bend[d]	energy[e]	net[f]
$^{14}C + HC/C + HC$	1.123[g]	0.928	0.960	0.997	1.000	0.998
	1.123[h]	0.928	1.019	0.999	1.105	1.077
$^{14}C + H^{14}C/C + HC$	1.250	0.866	0.932	0.993	1.000	1.003
	1.250	0.867	1.045	0.995	1.019	1.149
$Cl + {}^{14}CCl/Cl + CCl$	1.027	1.119	1.075	0.877	1.000	1.084
	1.027	1.119	0.988	0.878	1.002	0.999
$^{37}Cl + CCl/Cl + CCl$	1.048	0.973	0.986	0.996	1.000	1.002
	1.048	0.973	1.003	0.997	1.003	1.022
$^{37}Cl + C^{37}Cl/Cl + CCl$	1.077	0.959	0.980	0.992	1.000	1.005
	1.077	0.959	1.007	0.992	1.001	1.033
$^{14}C + H_2/C + H_2$	1.032	0.981	1.002	0.998	1.000	1.012
	1.032	0.981	1.007	0.998	1.003	1.020
$^{14}C + FH/C + FH$	1.151	0.918	0.979	0.991	1.000	1.026
	1.151	0.917	1.036	0.998	0.978	1.066
$Cl + {}^{14}CH/Cl + CH$	1.166	0.933	0.994	0.967	1.000	1.045
	1.166	0.930	1.071	0.977	0.973	1.103
$^{37}Cl + CH/Cl + CH$	1.022	0.986	0.993	0.999	1.000	1.000
	1.022	0.986	1.005	1.001	0.993	1.007
$^{37}Cl + HO/Cl + HO$	1.027	0.983	0.998	0.999	1.000	1.007
	1.027	0.983	0.999	1.000	0.999	1.007
$O + Cl^{14}C/O + ClC$	1.016	1.016	1.075	0.974	1.000	1.081
	1.016	1.020	1.076	0.970	1.001	1.081
$O + {}^{37}ClC/O + ClC$	1.016	1.014	0.998	0.976	1.000	1.003
	1.016	1.014	0.998	0.976	1.000	1.003
$^{37}Cl + {}^{37}ClH/Cl + ClH$	1.086	0.955	0.971	0.991	1.000	0.998
	1.086	0.954	0.971	0.992	1.000	0.998

[a-h] See Table V.

Table VII. Test of the Swain-Schaad Equation (6) at 300 and 600 K

reaction A + BC	T, K	$k_H^{\ddagger}/k_T^{\ddagger}$	$(k_H^{\ddagger}/k_T^{\ddagger})_{SS}$	k_H^{CVT}/k_T^{CVT}	$(k_H^{CVT}/k_T^{CVT})_{SS}$	$k_H^{CVT/SAG}/k_T^{CVT/SAG}$	$(k_H^{CVT/SAG}/k_T^{CVT/SAG})_{SS}$
C + HC	300	9.78	9.69	0.74	0.65	1.03	0.90
	600	3.47	3.44	0.90	0.86	0.98	0.93
O + HO	300	25.29	25.31	0.68	0.65	0.72	0.69
	600	5.33	5.32	0.86	0.84	0.87	0.86
C + HO	300	1.03	0.95	1.05	1.00	1.33	1.25
	600	1.07	1.05	1.08	1.07	1.15	1.13
Li + HO	300	6.56	6.52	6.01	5.93	6.17	6.08
	600	2.47	2.50	2.32	2.35	2.37	2.39
Cl + HO	300	1.60	1.61	1.45	1.45	1.54	1.53
	600	1.29	1.29	1.21	1.21	1.28	1.28
Li + HI	300	2.82	2.76	2.64	2.57	2.74	2.66
	600	1.62	1.61	1.46	1.44	1.43	1.41
I + HBr	300	1.34	1.34	1.31	1.31	1.40	1.40
	600	1.15	1.15	1.14	1.14	1.21	1.21

stretching degree of freedom for symmetric and nearly symmetric reactions; then the bend degree of freedom, which favors $k_D > k_H$, may become the determining factor. The present case provides an even more dramatic example than one might expect in general. In particular, in proceeding from the reactants to the canonical variational dividing surfaces, not only does the bending frequency increase more for ^1H than for ^2H, but also the stretching frequency decreases less. Thus, in this case, both degrees of freedom contribute to the prediction that, in the absence of tunneling, the isotope effect is inverse. Notice that, if the dividing surfaces for both isotopes had the same location, it would be impossible for the stretching entropic effect to favor $k_H < k_D$ (assuming, as is almost certainly the case, that the stretching force constant is less at the dividing surface than for reactants). The crucial new element of variational transition state theory is that we must consider force-constant changes and geometry changes as well as changes of mass.

The small isotope effects predicted by CVT for the symmetric hydrogen-atom transfers deserve some further comment because they seem to be contrary to some experimental experience. There are several considerations to keep in mind in this regard. The crucial point is that the present calculations show, for some potential-energy surfaces in the absence of tunneling corrections, that CVT predicts quite different KIEs than conventional transition state theory. The fundamental assumption of transition-state theory is that there is no recrossing of the transition state dividing surface. CVT actually locates the dividing surface which is dynamically crossed least (and therefore recrossed least), whereas conventional transition state theory locates this dividing surface by an a priori energetic criterion. Therefore CVT is a more consistent theory within the framework of equilibrium reaction rate theories. Therefore, even if conventional transition state theory might correlate some subset of experimental data more easily, one wants to explain why. The reasons for particular cases might be one or more of the following: (1) compensation of errors caused by the transition state theory treatment of quantal effects, especially tunneling; (2) real potential energy surfaces for some reactions being qualitatively different from those assumed here; (3) an incorrect mechanism being used to interpret some experimental results. Although it would be inappropriate to review the whole relevant literature here, we will next briefly

summarize the considerations relevant to points (1)–(3). We leave it to future work to make applications to specific systems.

(1) There is no proven theory available for treating tunneling in small-skew-angle systems. The vibrationally adiabatic ground state tunneling correction employed in this paper is known to generally underestimate the effect of tunneling. More accurate theories of tunneling have been proposed by Marcus and Coltrin[36] and Miller et al.[37] We have applied these theories to several of the cases studied here, and they generally predict more tunneling than the model used for the numerical results here. However, they do not lead to large changes in the predicted deuterium–protium KIEs for C + HC and O + HO. Thus we will not present these results here in detail. Although these newer methods are generally more reliable than the minimum-energy-path zero-curvature model used for tunneling here, they are probably not reliable for small-skew-angle systems.[38] For such systems the whole notion of treating the minimum-energy path as the reaction coordinate or as a zero-order reaction coordinate begins to break down. Thus in particular the treatment of degrees of freedom transverse to this path as adiabatic with respect to this path breaks down. Therefore the quantum numbers and quantized energies of the transverse stretch may be less meaningful for this kind of system than for the other systems treated here. In other words, we cannot separate tunneling (quantal effects on reaction coordinate motion) from classical and quantal manifestations of vibrational nonadiabaticity for this kind of system. Thus both conventional transition state theory and CVT suffer from particularly serious nonseparability of reaction-coordinate motion for small-skew-angle systems. Within the generalized transition state theory framework, however, CVT is probably to be preferred on theoretical grounds. First, it is more consistent with the fundamental no-recrossing assumption as discussed above. Second, it tends to locate the transition state dividing surface farther from the highest curvature part of the minimum-energy path and thus the breakdown of the nonseparability assumption should be less severe than for the conventional theory. Further work on quantal effects, both separable and nonseparable, is required to treat this kind of system with confidence. We are currently carrying out a test of the CVT for T + HD,[39] which is a small-skew-angle system for which tests against accurate quantal calculations are feasible. We hope that this and future work will lead to a better understanding of small-skew-angle systems.

(2) The set of potential-energy surfaces used here predicts large errors in conventional transition state theory for small-skew-angle systems. We have explored other semiempirical potential energies in unpublished work and the effects are sometimes greater and sometimes less than for BEBO surfaces. An ab initio study of the Cl + HCl system is underway,[40] and we hope that it will be more definitive, at least for Cl + HCl. The present study does indicate, however, that it is unsatisfactory to simply interpret the KIE by a model involving conventional transition state theory without questioning the stability of the treatment with respect to varying the location of the dividing surface for the particular potential-energy surface involved.

(3) Once it is recognized that symmetric saddle points do not have to lead to large KIEs for hydrogen or proton transfer, some experimental measurements of small KIEs that are interpreted in terms of more complicated mechanisms, e.g., additional metastable intermediates, might receive alternative interpretations in terms of simple symmetric barrier geometries. Then additional experiments or calculations might be required to make a definitive interpretation in particular cases.

Conventional TST for H-atom transfers predicts a minimum primary H/D isotope effect for a very asymmetric (reactant-like or product-like) transition state and a maximum isotope effect for a very symmetric transition state. We have just seen that canonical variational theory predicts a small isotope effect for the present BEBO potential energy surfaces for symmetric reactions like C + HC and O + HO. Notice, however, that the prediction occurs because the variational state is not symmetric. For the symmetric choice of dividing surface these potential-energy surfaces exhibit the usual prediction for the isotope effect. The Melander–Westheimer correlation of small isotope effects and asymmetric transition states is so commonly applied that this result is very important. Such correlations, which are widespread in the literature, may require reinterpretation. In particular the implication of a small isotope effect may be that the variational transition state (free-energy maximum) is asymmetric, as opposed to the usual interpretation that the conventional transition state (classical potential energy maximum) is asymmetric. The point most worth emphasis is not the fact that the present BEBO formalism for potential-energy surfaces leads to small canonical variational isotope effects for the particular reactions C + HC and O + HO, but rather that there exist realistic potential surfaces and mass combinations such that canonical variational theory predicts a small isotope effect even when the maximum in the classical potential energy along the reaction coordinate occurs at a symmetric position. There exist other cases, e.g., the H + H_2 reaction on the surface of Porter and Karplus,[41] where the canonical variational theory predicts the same isotope effect for perdeuteration at 300 K as does conventional transition state theory. Thus there also exist cases where the deviation of the prediction of canonical variational theory from conventional transition state theory is quantitatively important but less dramatic than for the present surface for C + HC.

The ^{14}C isotope effect for the C + HC reaction is also sensitive to variational location of the dividing surface. Table IV shows that at the saddle point ω_e is 46 cm^{-1} higher for $^{12}C^1H^{12}C$ than for $^{14}C^1H^{14}C$. The difference in reactants is only 16 cm^{-1}; therefore, the ^{14}C reaction is faster according to conventional transition state theory. However, at the variational transition states for 600 K, ω_e is actually 20 cm^{-1} lower for the ^{12}C isotope. This reverses the direction of the predicted isotope effect (see Table II).

Although it is not a symmetric system, C + H_2 shows effects which are analogous to those for C + HC. See, e.g., Figure 3 and Table IV. Tables I and IV show that at low temperature conventional transition state theory predicts a normal isotope effect with protium reacting faster than deuterium because of the larger zero-point energy of reactants and hence the larger release of stretching energy for the protium case. However, the same factor, the larger stretching frequencies for the protium reaction, also allows for a greater diminution of the calculated rate when the dividing surface is varied and thus allows canonical variational theory to decrease the predicted isotope effect. In C + H_2, unlike C + HC, the translational partition function makes an important contribution to the isotope effect; it contributes 2.31 to k_H/k_D at any temperature. At low temperature, Table I shows that the net effect of vibrations and rotations is to increase k_H/k_D in the conventional theory. In particular the stretching, bending, and rotational degrees of freedom contribute factors of 2.36, 0.45, and 1.10. But in canonical variational theory k_H/k_D is less than 2.31. The contributions to the net KIE of 1.7 at 600 K are as follows: translation, 2.31; stretch, 1.27; bend, 0.45; rotation, 1.12; classical potential energy, 1.17. Clearly the variational effect upon the KIE is dominated by competition between the stretching entropic effect and the classical potential energy. The prediction of the ^{14}C KIE is most sensitive to variational optimization of the dividing surface location at low temperature; e.g., at 300 K such variational optimization changes the predicted KIE from 1.013 to 1.029 (with a further change to

1.027 when the semiclassical adiabatic ground-state transmission coefficients are included). The change in the heavy-atom KIE comes about because $k^{\ddagger}/k^{CVT}$ is 7.94 for ^{12}C but increases to 8.07 for ^{14}C. This is a change of 1.6% and so the heavy-atom KIE changes by 1.6%. It is clear that small KIEs are particularly vulnerable to this kind of change.

The KIEs for multiply substituted species can be used to test the rule of the geometric mean.[15] Table II shows that for the C + H_2 reaction the ^{14}C KIEs predicted by canonical variational theory are much more sensitive to deuterium substitution than are the ^{14}C KIEs predicted by conventional transition state theory. This is a direct consequence of the change in geometrical structure and force constants upon deuterium substitution. This kind of multiple isotopic substitution, by testing the assumptions of the law of the geometric mean, can provide a rather direct test of whether the free energy of activation for the effective transition state for a given reaction is drastically different for two isotopic transition states.

From the preceding discussion it is clear that the effects of the different degrees of freedom upon the KIEs can be interpreted in terms of five factors involving the ratios of relative translational partition functions, rotational partition functions, stretching partition functions, bending partition functions, and Boltzmann factors for the two isotopes. These ratios are summarized for some of the deuterium KIEs in Table V and for some of the heavy-atom KIEs in Table VI for both conventional and canonical variational transition state theory at 600 K. Tables V and VI are arranged with the systems with the most symmetrical locations of the saddle points listed first.

Tables V and VI provide an overall view and a survey of the effects, so we will limit our discussion to pointing out the few most important trends. Table V shows that for symmetric or nearly symmetric systems the major contribution to the deuterium KIE comes from the stretching degree of freedom in conventional TST. However, variational relocation of the dividing surface decreases this contribution. For the reactions with very asymmetric saddle points the contribution from the stretching degree of freedom is affected only slightly by variationally locating the dividing surface. For intermediate cases the effect upon the contribution from the stretch to the KIE is also intermediate. In these examples contributions to the KIEs from rotations always favor $k_H > k_D$ and contributions to the KIEs from bends always favor $k_H < k_D$. Variational location of the dividing surface has negligible effect upon these ratios. Thus the variational effects to deuterium isotope effects are dominated by competition between energetic and stretching entropic effects as a general rule.

Table VI shows that for heavy-atom KIEs for symmetric or near-symmetric systems the effect upon the ratio of stretching partition functions of variational optimization of the dividing surface is just the opposite of that found for deuterium KIEs. Again the ratios of rotational partition functions and bending partition functions are changed very little by the variational procedure.

In summary we see that the effect upon the KIEs of variational optimization of the dividing surface is dominated by the stretching degree of freedom. Since the variational effects upon the stretching degree of freedom are most pronounced for systems with symmetric and nearly symmetric saddle points we find that the variational effects upon the KIEs are also most pronounced for such systems.

Since the original formulation of the Swain–Schaad equation, the conditions for its validity, especially in the presence of tunneling, have been carefully analyzed in the context of conventional transition state theory.[42-44] Table VI is an attempt to learn whether the equation still holds approximately true when the generalized transition state is relocated variationally for each isotope. Table VII shows that the Swain–Schaad equation predicts canonical variational k_H/k_T values quite well from canonical variational k_H/k_D values for all systems tested here. Without or with the tunneling correction, its predictions hold only slightly less well than in conventional transition state theory. Another way to test the Swain–Schaad equation is to use both k_H/k_D and k_H/k_T to calculate the exponent and to see how close the exponent comes to 1.44. The equation fares much more poorly on that kind of test, especially for C + HC, O + HO, and C + HO.

VI. Concluding Remarks

Although kinetic isotope effects involve a ratio of rate constants, the present article shows that canonical variational theory sometimes predicts quite different isotope effects than conventional transition state theory for realistic potential-energy surfaces. Prediction of isotope effects for real systems, as opposed to the present study of isotope effects for BEBO potential-energy surfaces, requires a careful consideration of the accuracy of the potential-energy surface. However, the BEBO surfaces are realistic enough that the same kinds of differences in isotope-effect predictions seen in this work should be expected to occur also for some real systems.

The present results have very important implications for the theory of kinetic isotope effects. Kinetic isotope effects are almost universally interpreted in terms of conventional transition state theory. This theory involves the simplifying feature that the geometry and force constants of the transition state are the same for all isotopic variants of a reaction. The present calculations show, however, that, when a generalized transition state is defined and its location determined variationally, the location is sometimes strongly dependent on isotopic substitution. Thus one must consider not only variations of masses but also variations of force constants and bond distances in calculating the partition functions for the generalized transition states. This considerably complicates the theory and the interpretation of experimental results. This is especially true when one tries to use kinetic isotope effects as an indication of structure, in particular when one tries to relate kinetic isotope effects to the structure of a saddle point on a potential-energy surface. The conventional transition state theory of kinetic isotope effects is so elegant and successful at the empirical correlation of data that one is almost regretful to find out that a better theory shows up some inadequacies. Future progress will require considering a wider range of reaction types and potential energy surface types and also developing a more reliable way to estimate tunneling and nonseparability effects. It would also be useful to estimate recrossing effects more accurately. One way to do this is by considering less constrained variational optimizations of the location of the dividing surface.[19]

Acknowledgments. The authors are grateful to Professor Maurice M. Kreevoy for helpful discussions. This work was supported in part by the National Science Foundation (Quantum Chemistry Program) under Grant CHE 77-27415 and by the U.S. Department of Energy (Division of Chemical Sciences, Office of Basic Energy Sciences) through Contract No. DE-AC02-79ER10425.

References and Notes

(1) J. Bigeleisen and M. Wolfsberg, *Adv. Chem. Phys.*, **1**, 15 (1958).
(2) L. Melander, "Isotope Effects on Reaction Rates", Ronald Press, New York, 1960.
(3) "Isotope Effects in Chemical Reaction Rates", *ACS Monogr.* **No. 167** (1970). The general theory is well covered in the chapters by W. A. Van Hook and by E. K. Thornton and E. R. Thornton.
(4) E. Buncel and C. C. Lee, Ed., "Isotopes of Organic Chemistry", Vol. 2, Elsevier, Amsterdam, 1976.
(5) B. C. Garrett and D. G. Truhlar, *J. Phys. Chem.*, **83**, 1079 (1979), erratum in press. For a review, see D. G. Truhlar, *ibid.*, **83**, 188 (1979).
(6) B. C. Garrett and D. G. Truhlar, *J. Am. Chem. Soc.*, **101**, 4534 (1979).
(7) B. C. Garrett and D. G. Truhlar, *J. Am. Chem. Soc.*, **101**, 5207 (1979).
(8) M. M. Kreevoy in ref 4, p 1.

(9) K. T. Leffek in ref 4, p 89.
(10) C. H. Bamford and C. F. H. Tipper, Ed., "Comprehensive Chemical Kinetics", Vol. 8, Elsevier, Amsterdam, 1977. See especially the chapters by A. V. Willi, p 1, and F. Hibbert, p 97.
(11) W. A. Van Hook in ref 3, p 1.
(12) E. S. Lewis in ref 4, p 127.
(13) D. G. Truhlar and R. E. Wyatt, *Annu. Rev. Phys. Chem.*, **27**, 1 (1976); D. G. Truhlar, A. Kuppermann, and J. Dwyer, *Mol. Phys.*, **33**, 683 (1977).
(14) F. H. Westheimer, *Chem. Rev.*, **61**, 265 (1961).
(15) E. K. Thornton and E. R. Thornton in ref 3, p 213.
(16) Additional references are given in G. Brunton, D. Griller, L. R. C. Barclay, and K. U. Ingold, *J. Am. Chem. Soc.*, **98**, 6803 (1976).
(17) A. Fry in ref 3, p 364.
(18) A. Maccoll, *Annu. Rep. Prog. Chem., Sect. A*, **71**, 77 (1974).
(19) B. C. Garrett and D. G. Truhlar, *J. Phys. Chem.*, **83**, 1052, 3058E (1979).
(20) E. P. Wigner, *Trans. Faraday Soc.*, **34**, 29 (1938).
(21) W. H. Miller, *J. Chem. Phys.*, **62**, 1899 (1975); P. Pechukas in "Dynamics of Molecular Collisions", Part B, W. H. Miller, Ed., Plenum Press, New York, 1976, p 269.
(22) J. C. Keck, *Adv. Chem. Phys.*, **13**, 85 (1967).
(23) See, e.g., ref 13 and especially S. Chapman, B. C. Garrett, and W. H. Miller, *J. Chem. Phys.*, **63**, 2710 (1975).
(24) B. C. Garrett and D. G. Truhlar, *J. Phys. Chem.*, **83**, 200, 3058E (1979).
(25) A. Kuppermann, *J. Phys. Chem.*, **83**, 177 (1979).
(26) B. C. Garrett and D. G. Truhlar, *J. Phys. Chem.*, **83**, 2921 (1979).
(27) H. S. Johnston and C. A. Parr, *J. Am. Chem. Soc.*, **85**, 2544 (1963).
(28) S. W. Mayer, L. Schieler, and H. S. Johnston, *J. Chem. Phys.*, **45**, 385 (1966).
(29) See, e.g., A. R. Miller, *J. Am. Chem. Soc.*, **100**, 1984 (1978).
(30) B. C. Garrett and D. G. Truhlar, *J. Phys. Chem.*, **83**, 1915 (1979).
(31) C. G. Swain, E. C. Stivers, J. F. Reuwer, Jr., and L. J. Schaad, *J. Am. Chem. Soc.*, **80**, 5835 (1958).
(32) D. G. Truhlar and A. Kuppermann, *Chem. Phys. Lett.*, **9**, 269 (1971).
(33) D. G. Truhlar and A. Kuppermann, *J. Chem. Phys.*, **56**, 2232 (1972).
(34) D. G. Truhlar, A. Kuppermann, and J. T. Adams, *J. Chem. Phys.*, **59**, 395 (1973).
(35) The skew angle is defined as the angle between the asymptotic reactant and product channels when the potential energy for collinear geometries is plotted in coordinates in which the kinetic energy is a sum of square terms (no cross term). See ref 7 for further discussion and references.
(36) R. A. Marcus and M. E. Coltrin, *J. Chem. Phys.*, **67**, 2609 (1977).
(37) W. H. Miller, N. C. Handy, and J. E. Adams, *J. Chem. Phys.*, **72**, 99 (1980).
(38) For further discussion, see R. A. Marcus in "Physicochemical Hydrodynamics", Vol. 1, D. B. Spalding, Ed., Advance Publications, Guernsey, 1978, p 473; R. A. Marcus, *J. Phys. Chem.*, **83**, 204 (1979).
(39) B. C. Garrett, D. G. Truhlar, R. Grev, and R. B. Walker, work in progress.
(40) T. H. Dunning, A. F. Wagner, D. G. Truhlar, B. C. Garrett, and A. Magnuson, work in progress.
(41) R. N. Porter and M. Karplus, *J. Chem. Phys.*, **40**, 1105 (1964).
(42) J. Bigeleisen in "Tritium in the Physical and Biological Sciences", Vol. 1, International Atomic Energy Agency, Vienna, 1962, p 161.
(43) E. S. Lewis and J. K. Robinson, *J. Am. Chem. Soc.*, **90**, 4337 (1968).
(44) M. J. Stern and P. C. Vogel, *J. Am. Chem. Soc.*, **93**, 4664 (1971).

Cleaving CC Bonds in Cyclopropenium Ions

Eluvathingal D. Jemmis and Roald Hoffmann*

Contribution from the Department of Chemistry, Cornell University, Ithaca, New York 14853. *Received September 19, 1979*

Abstract: A cyclopropenium ion breaking one of its carbon–carbon bonds furnishes an orbital template which can be exploited by sundry mononuclear and binuclear transition metal fragments.

One of the many things that transition-metal complexes do, and we wish we knew better how to control it, is to cleave and form carbon–carbon bonds. In this paper one very specific CC bond breaking, that in cyclopropenium cations and cyclopropenones, is investigated theoretically. The case is special, but the theoretical methodology developed here lends itself to obvious extension.

We chose these three-membered rings for study in part because we understand the electronic structure of the organic moiety well and in part because the body of structural information on C_3R_3 and cyclopropenone complexes is just reaching the critical stage, revealing a continuum of bonding modes which may trace out a reaction coordinate for the insertion reaction.

The intrusion of a metal atom, with its associated ligands, into a CC bond of a strained three-membered ring may occur in either a single oxidative step, as in eq 1,[1] or following prior coordination of the organic ligand. Equation 2 represents perhaps the best characterized instance of this sequence.[2,3]

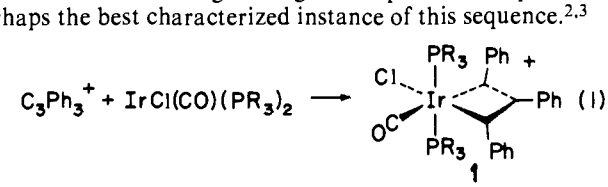

1

If coordination of the ring is a likely initial step, one is led to think about the ways in which a three-membered ring may be bound. Cyclopropenium complexes are not common, but we do have available structures in which the ring is η^3, **3**,[4-8] η^2, **4**,[9] and η^1, **5**.[10]

On the completely ring-opened or metallocyclobutadiene side we have the previously mentioned complexes **1** (and an analogous $RhCl_2(PMe_2Ph)_2(C_3Ph_3)$[12]) and **2**. Then we encounter a fascinating group of bi- or polynuclear complexes with C_3R_3 or C_2R_2CO units sitting atop them (**6**,[13] **7**,[14] **8**,[15] **9**,[16] and **10**[17]).

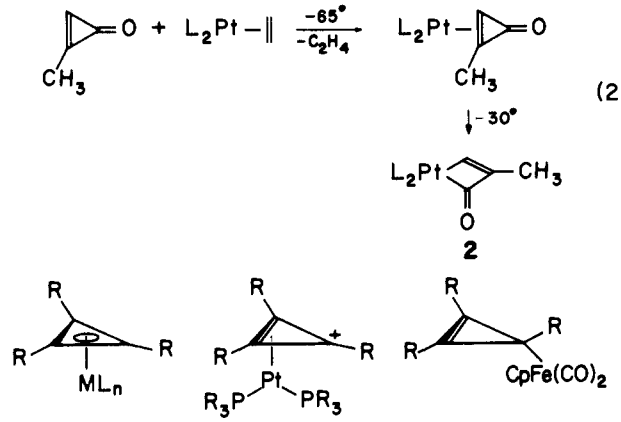

Are the three-membered rings in these complexes completely or only partially opened up? As the cyclopropenium ring is cleaved one CCC angle, θ, opens up and the CC bond opposite, R, stretches. Less obvious, but important, is the fact that the orientation of the metal atom relative to the three-carbon plane changes. The metal is perpendicular to the plane

0002-7863/80/1502-2570$01.00/0